Chem

CellPress

Article

A Highly Porous Metal-Organic Framework System to Deliver Payloads for Gene Knockdown

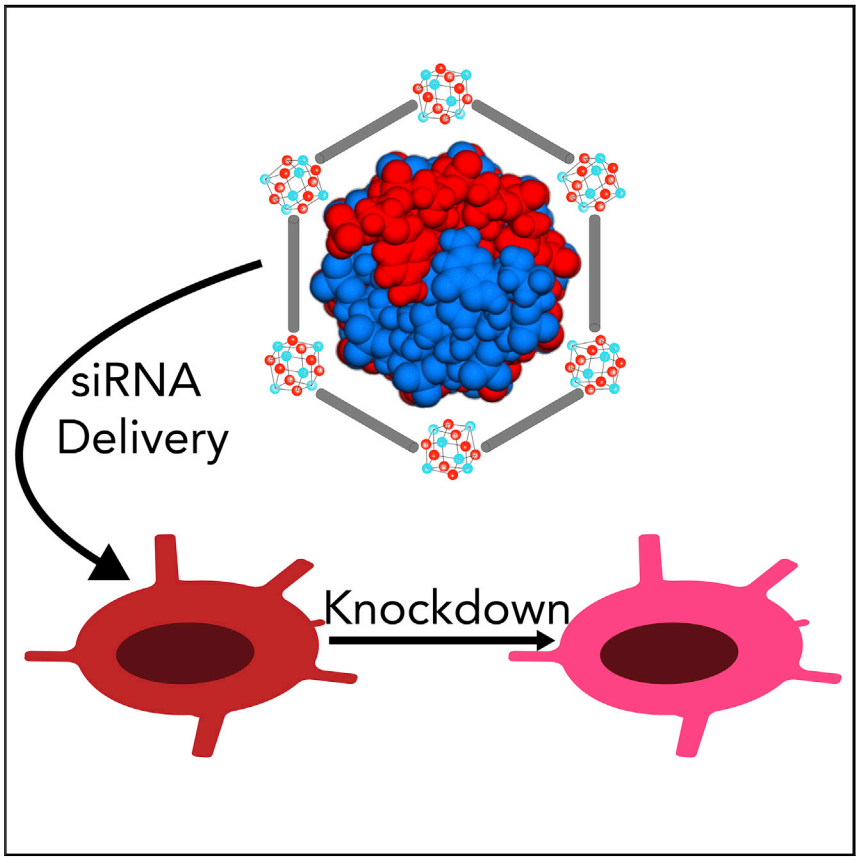

Gene knockdown is an advantageous therapeutic strategy to lower dangerous genetic over-expression. However, the molecules responsible for initiating this process are unstable. Porous nanoparticles called metal-organic frameworks can encapsulate, protect, and deliver these compounds efficaciously without the need for chemical modifications—commonly done to enhance stability. By applying this platform technology, this work demonstrates the successful reduction in expression of a gene by avoiding retention and subsequent degradation in cellular compartments.

Michelle H. Teplensky, Marcus Fantham, Chetan Poudel, ..., Gabriele Kaminski Schierle, Clemens F. Kaminski, David Fairen-Jimenez

cfk23@cam.ac.uk (C.F.K.)
df334@cam.ac.uk (D.F.-J.)

HIGHLIGHTS

Biodegradable MOF used to encapsulate and protect native siRNA from degradation

Delivered system avoids endosomal retention and knocks down gene expression

Structured illumination microscopy used to study endocytic uptake

Teplensky et al., Chem 5, 1–16
November 14, 2019
https://doi.org/10.1016/j.chempr.2019.08.015

Please cite this article in press as: Teplensky et al., A Highly Porous Metal-Organic Framework System to Deliver Payloads for Gene Knockdown, Chem (2019), https://doi.org/10.1016/j.chempr.2019.08.015

Chem

CellPress

Article

A Highly Porous Metal-Organic Framework System to Deliver Payloads for Gene Knockdown

Michelle H. Teplensky,[1] Marcus Fantham,[2] Chetan Poudel,[2] Colin Hockings,[3] Meng Lu,[3] Alina Guna,[4] Marta Aragones-Anglada,[1] Peyman Z. Moghadam,[1,5] Peng Li,[6] Omar K. Farha,[6,7] Sandra Bernaldo de Quirós Fernández,[8] Frances M. Richards,[8] Duncan I. Jodrell,[8] Gabriele Kaminski Schierle,[3] Clemens F. Kaminski,[2,*] and David Fairen-Jimenez[1,9,*]

SUMMARY

Since first reported, RNA interference (RNAi) has become a widely used tool for cellular genetic knockdown. However, RNA instability and susceptibility to enzymatic degradation have prevented its widespread clinical use. Thus, research efforts are seeking methods to protect the fragile RNA payload during delivery. Here, we report the use of a metal-organic framework (MOF) to load, protect, and deliver small interfering ribonucleic acids (siRNAs). We confirmed the protection of MOF-internalized siRNA from enzymatic degradation. Furthermore, through combined encapsulation of siRNA in the MOF with various cofactors (proton sponge, KALA peptide, and NH_4Cl), we show that endosomal retention can be evaded and ensure that gene knockdown is efficacious. *In vitro* studies after siRNA-MOF complexation demonstrated up to 27% consistent knockdown. We use structured illumination microscopy (SIM) to study the complex's endocytic uptake. Overall, we demonstrate the potential of these highly porous and biodegradable materials to improve the efficacy and efficiency of future gene therapies.

INTRODUCTION

Every year, more than 14 million people are diagnosed with cancer, and more than 1 in 3 people will develop some form of cancer during their lifetime.[1,2] Although there are great advances in terms of diagnosis and treatment, cancer remains a key societal health concern. Depending on cancer type and stage, common treatments include surgical resection and chemo- and radiotherapy.[3] The key to the success of these treatments lies in early detection, screening, and improvements in the treatment technologies.[4] In many cases, however, complete tumor resection is not feasible due to the invasive nature of required procedures, making local recurrence inevitable. In addition, many patients are not suitable for surgery due to comorbidities or proximity of tumors to vital structures. This is particularly critical for hard-to-treat cancers such as ovarian cancer, malignant mesothelioma, triple-negative breast cancer, and pancreatic cancer—where 5-year survival rates have not improved in the last 20 years and are still around 10%.[5,6] For these cancers, common treatments are not successful, and there is an imperative need to develop novel therapeutic approaches.

One such approach is the use of small interfering ribonucleic acids (siRNAs) for gene knockdown expression of key cancer driver genes, which has received great

The Bigger Picture

Strategies to treat cancer have expanded since the discovery of small interfering ribonucleic acids (siRNAs). This approach allows for selective high-efficiency knockdown of cancer-causing genes. However, because siRNA is inherently unstable and prone to enzymatic degradation, chemical modifications are often used. Modifications can affect knockdown efficacy and have to be changed for each sequence. In this regard, highly porous metal-organic frameworks (MOFs) offer a platform for the encapsulation of unmodified, native siRNA, which is then protected from enzymatic degradation. We report the successful encapsulation and delivery of protected native siRNA. We complex the siRNA-MOF system with additional cofactors that promote escape from cellular vesicles and allow it to reach the cytosol and successfully knock down a gene. By applying this platform to clinically relevant genes, the potential exists to use any native siRNA sequence and achieve potent endosomally evasive therapy.

Please cite this article in press as: Teplensky et al., A Highly Porous Metal-Organic Framework System to Deliver Payloads for Gene Knockdown, Chem (2019), https://doi.org/10.1016/j.chempr.2019.08.015

attention over recent years.[7–9] This method is attractive because it (1) has a high efficiency of knockdown, (2) is highly specific and thus exhibits minimal off-target effects, and (3) has a lack of systemic toxicity and immunoreactivity.[10] Various medical diseases, in addition to cancer, including neurological disorders and viral infections, may benefit in the future from siRNA gene therapies.[11,12] siRNA is a double-stranded RNA fragment typically 21–23 nt in length that can code for a particular cellular gene, cleaved from endogenously expressed long double-stranded RNAs (dsRNAs).[13] Synthetically created siRNAs have potential as inhibitors of various disease-associated genes, bypassing the first step of endogenous cleavage and allowing for the creation of a platform technology with any genetic sequence. The mechanism for siRNA delivery and subsequent gene knockdown is universal for any selected sequence, giving it targeted therapeutic potential.[11] This is in contrast to drugs currently used in cancer therapies—including doxorubicin, 5-fluorouracil, or docetaxel—that may act on multiple pathways.[14]

Although siRNA therapy has the potential to benefit patients with cancer, the main limitation is its lack of stability and ease of degradation by native biological enzymes.[15,16] In addition, while non-encapsulated small-molecule drugs can enter the cell cytoplasm directly through the plasma membrane, macromolecule delivery into the cytoplasm is challenging. To overcome this problem, researchers have altered the chemical structure of siRNAs through modifications to the phosphodiester or sugar backbone or have changed bases in the sequence.[17,18] There has been some success with chemical modifications to siRNAs,[19,20] such as improving duplex stability and conferring nuclease resistance by replacing the 2′-hydroxyl of the ribose; modification of a few residues has been generally well tolerated.[21] However, chemical modifications are sequence dependent and can require tailoring for different siRNAs. Additionally, chemical modification tends to lower the therapeutic efficacy of the siRNAs upon cytosolic delivery. An alternative approach is the incorporation, and thus protection, of siRNAs as a payload within polymers or nanoparticles.[22–24] Some examples are organic delivery vehicles, such as liposomes or nanoparticles, that carry siRNAs into the cell, protecting them from degradation in the extracellular space. However, liposomes tend to accumulate in the reticuloendothelial system,[16] and some formulations of nanoparticles can only achieve low loading capacities due to the low negative charge and intrinsic stiffness of double-stranded siRNA.[22,25,26]

In this context, metal-organic frameworks (MOFs), a class of porous self-assembled materials composed of metal ions or clusters connected by organic linkers, are one of the most promising materials for biomedicine.[27–31] There are currently more than 84,000 MOF structures in the Cambridge Structural Database and the diversity that MOFs offer is of particular interest for siRNA delivery. Others have utilized MOFs for the delivery of siRNAs and other biomacromolecules, such as CRISPR/Cas9 machinery.[29,32,33] However, in these cases, the selected biocompatible MOFs do not contain pore dimensions large enough to allow for internally adsorbed siRNAs.[29,33] Additionally, in the case with CRISPR/Cas9, the synthesis had to be altered to build the framework (ZIF-8) around the biomacromolecule machinery,[32] limiting in principle the scope of frameworks feasible with this method, as well as incorporating a zinc-based moiety that has been shown in literature to be toxic even at low concentrations.[34] By selecting appropriate MOFs that can provide large pore sizes, we allow for the encapsulation of macromolecules and their subsequent protection, increasing their bioavailability within the tumor while avoiding off-target toxicity.[27] Among the different MOFs, we and others have utilized zirconium-based MOFs (Zr-MOFs) for a variety of reasons.[35,36] They have been shown to be stable in water, a useful characteristic for loading the MOFs with a biological payload, and

[1]Adsorption & Advanced Materials Laboratory (AAML), Department of Chemical Engineering & Biotechnology, University of Cambridge, Philippa Fawcett Drive, Cambridge CB3 0AS, UK

[2]Laser Analytics Group, Department of Chemical Engineering & Biotechnology, University of Cambridge, Philippa Fawcett Drive, Cambridge CB3 0AS, UK

[3]Molecular Neuroscience Group, Department of Chemical Engineering & Biotechnology, University of Cambridge, Philippa Fawcett Drive, Cambridge CB3 0AS, UK

[4]MRC Laboratory of Molecular Biology, Cambridge CB2 0QH, UK

[5]Department of Chemical and Biological Engineering, University of Sheffield, Mappin Street, Sheffield S1 3JD, UK

[6]Department of Chemistry, Northwestern University, Evanston, IL 60208, USA

[7]Department of Chemical and Biological Engineering, Northwestern University, Evanston, IL 30208, USA

[8]Cancer Research UK, Cambridge Institute, University of Cambridge, Cambridge CB2 0RE, UK

[9]Lead Contact

*Correspondence: cfk23@cam.ac.uk (C.F.K.), df334@cam.ac.uk (D.F.-J.)

https://doi.org/10.1016/j.chempr.2019.08.015

Please cite this article in press as: Teplensky et al., A Highly Porous Metal-Organic Framework System to Deliver Payloads for Gene Knockdown, Chem (2019), https://doi.org/10.1016/j.chempr.2019.08.015

demonstrate a lack of toxicity and high thermal, mechanical, and chemical stabilities.[37–39] Importantly, however, these MOFs lack long-term stability in biological solvents where their breakdown prevents potentially *in vivo* accumulation.[31] In this work, we bring together a combination of multidisciplinary tools to develop a MOF-based platform for the encapsulation of siRNAs and its successful delivery into cells. We explore the mechanism through which the MOF is able to protect the siRNA from degradation in the extracellular space and also how the siRNA is released from the MOF and delivered to the cytosol to become active in the cell. We also prove that the system leads to the specific knockdown of a targeted gene.

RESULTS AND DISCUSSION

Design of Cell System and Corresponding siRNAs

We utilized a previously designed HEK293 cell line[40] (referred to here as HEK293-mC) based on the commercially available T-REx Flp-In system, where mCherry fluorescence expression can be induced using doxycycline or tetracycline (dox or tet). To coordinate an siRNA sequence with the mCherry gene genetically engineered into the HEK293-mC cells, we designed a custom siRNA sequence. We sought a sequence that limited off-target effects and effectively coded for the inducibly expressed mCherry protein. From the genetic code of the mCherry used, 5 out of 32 21-nt length sequences were identified as promising candidates due to their low GC content (<50%) and no stretches of greater than 4 T or A base pairs, as literature demonstrated these considerations improve activity.[41,42] We evaluated these 5 siRNAs loaded in lipofectamine qualitatively using microscopy and western blot analysis to determine whether there was any knockdown in intracellular mCherry signal; Table S1 lists the 5 identified siRNAs. Figure 1A shows optical microscopy images of 4 siRNA control conditions after they are incubated with HEK293-mC cells, some of which are doxycycline induced; Figure S1 shows the quantitative intensity analysis of the microscope images. When not induced (i.e., −dox in Figure 1A), the cells show no visible fluorescence, whereas when induced (i.e., +dox) and not siRNA treated ("no treatment"), the cells fluoresce. To demonstrate that only a specific targeted siRNA sequence leads to knockdown of the mCherry fluorescence, we used a "scrambled siRNA." Differences in brightness levels between cells treated with scrambled siRNAs and those with no treatment were not significant, verifying that the random sequence has no effect on mCherry knockdown. When reverse transfecting the 5 different custom siRNAs with the cells in Figure 1B, the brightness of the red signal varies between different siRNA strands. This indicates that siRNA 2, 3, 17, 28, and 29 had differential knockdown efficiencies for mCherry, with siRNA 3 and 28 appearing to be most effective. This is clear in the western blot (Figure 1C), where bands for anti-red fluorescent protein (RFP) antibody for samples 3 and 28 are noticeably less intense than any other band of mCherry-induced cells. A Ponceau stain shows equal loading of all samples (Figure 1D). For all subsequent experiments, we utilized siRNA sample 3 as a double-stranded sequence with the sense strand 5′-AAGGAGTTCATGCGCTTCAAG -3′.

Loading of siRNAs into MOF and Characterization

In order to select an optimal Zr-MOF, we performed molecular simulations to find a structure with a porosity compatible with this specific macromolecule; this also allows us to gain insights into how the presence of one double-stranded siRNA 3 molecule affects the energetics of the encapsulating MOF system. We considered NU-1000 (Zr_6-based MOF composed of $Zr_6(\mu 3\text{-}OH)_4(\mu_3\text{-}O)_4(OH)_4(OH_2)_4$ nodes and pyrene-based linkers [$TBAPy^{4-}$, 1,3,6,8-tetrakis(p-benzoate)pyrene];[43] NU: Northwestern University) based on previous experience and the possibility of tuning the particle size into the nm range (which we term nNU-1000). We have previously performed

Please cite this article in press as: Teplensky et al., A Highly Porous Metal-Organic Framework System to Deliver Payloads for Gene Knockdown, Chem (2019), https://doi.org/10.1016/j.chempr.2019.08.015

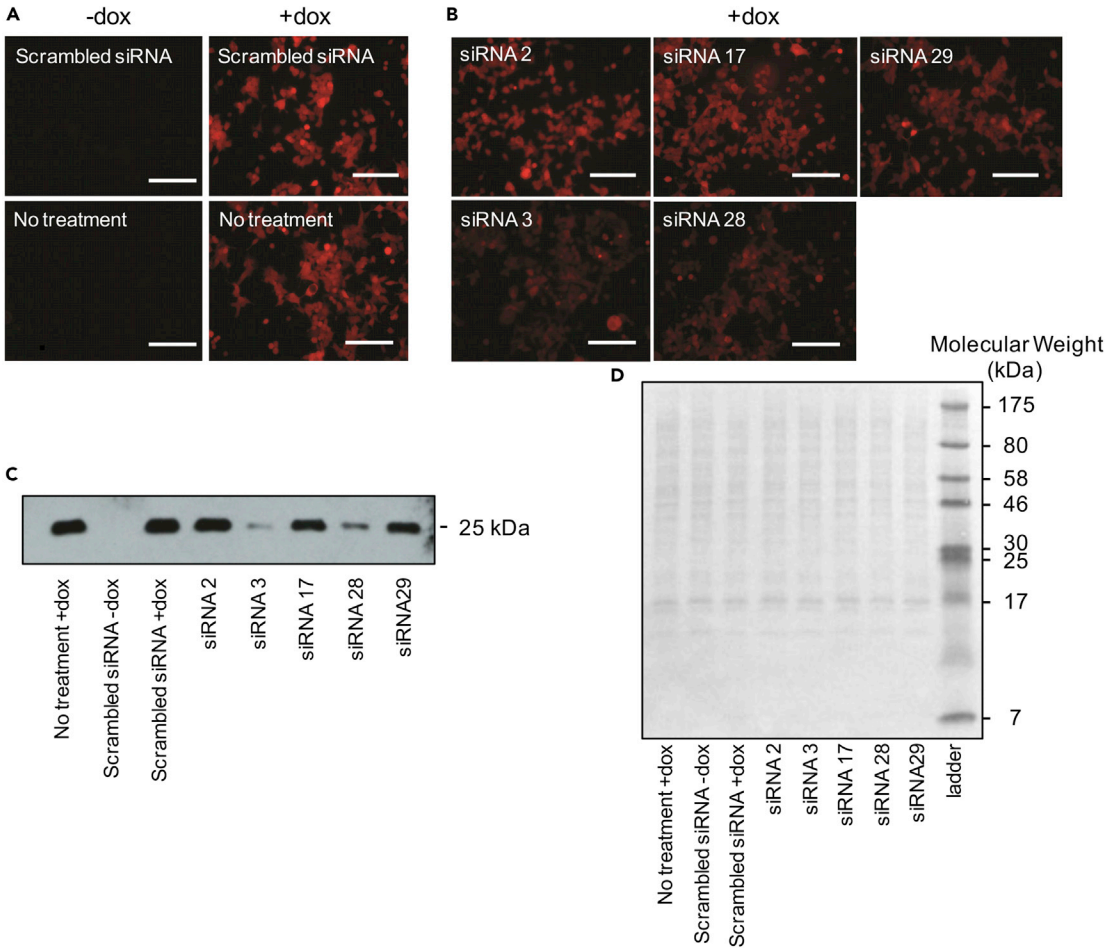

Figure 1. siRNA Design and Testing on Doxycycline-Induced HEK293-mC Cells

(A) Optical microscopy of HEK293 T-Rex Flp-In-mCherry cells when induced with doxycycline (+dox) and when not induced with doxycycline (−dox) for cells under treatment with scrambled siRNA (top) or without any siRNA (bottom) and lipofectamine. Scale bar, 100 μm.

(B) Corresponding images of doxycycline-induced cells (+dox) transfected with five different siRNA sequences coding for the mCherry gene. Scale bar, 100 μm.

(C) Western blot using anti-RFP antibody for the same conditions as depicted in (A) and (B). Bands represent relative levels of mCherry protein within cells post-transfection.

(D) Ponceau stain evaluating equal effectiveness of loading.

cell toxicity assessments and degradation studies in phosphate-buffered saline (PBS) for this particular MOF, which verify its biocompatibility and use for these biological applications.[31] We have also verified by proton NMR that the N,N-dimethylformamide (DMF) used during the solvothermal synthesis of the MOF, which could negatively impact future biological applications, is completely removed during the purification and activation of the MOF (Figure S2). Additionally, the porosity of nNU-1000 is sufficiently large to allow the encapsulation of siRNA 3 within its 3 nm diameter and hexagonal mesoporous channels. Figure 2A shows an energy minimized final configuration of an siRNA molecule in nNU-1000 pore model, with a favorable binding energy of −878 kJ/mol; the energies of nNU-1000 with siRNA compared with the isolated systems are located in Table S2. It indicates that there is sufficient free volume for the siRNA and NU-1000 components to pack without distortions as is verified with the favorable (negative) energy, suggesting a thermodynamic preference for the siRNA molecule to be located inside the NU-1000 pore channel.

Please cite this article in press as: Teplensky et al., A Highly Porous Metal-Organic Framework System to Deliver Payloads for Gene Knockdown, Chem (2019), https://doi.org/10.1016/j.chempr.2019.08.015

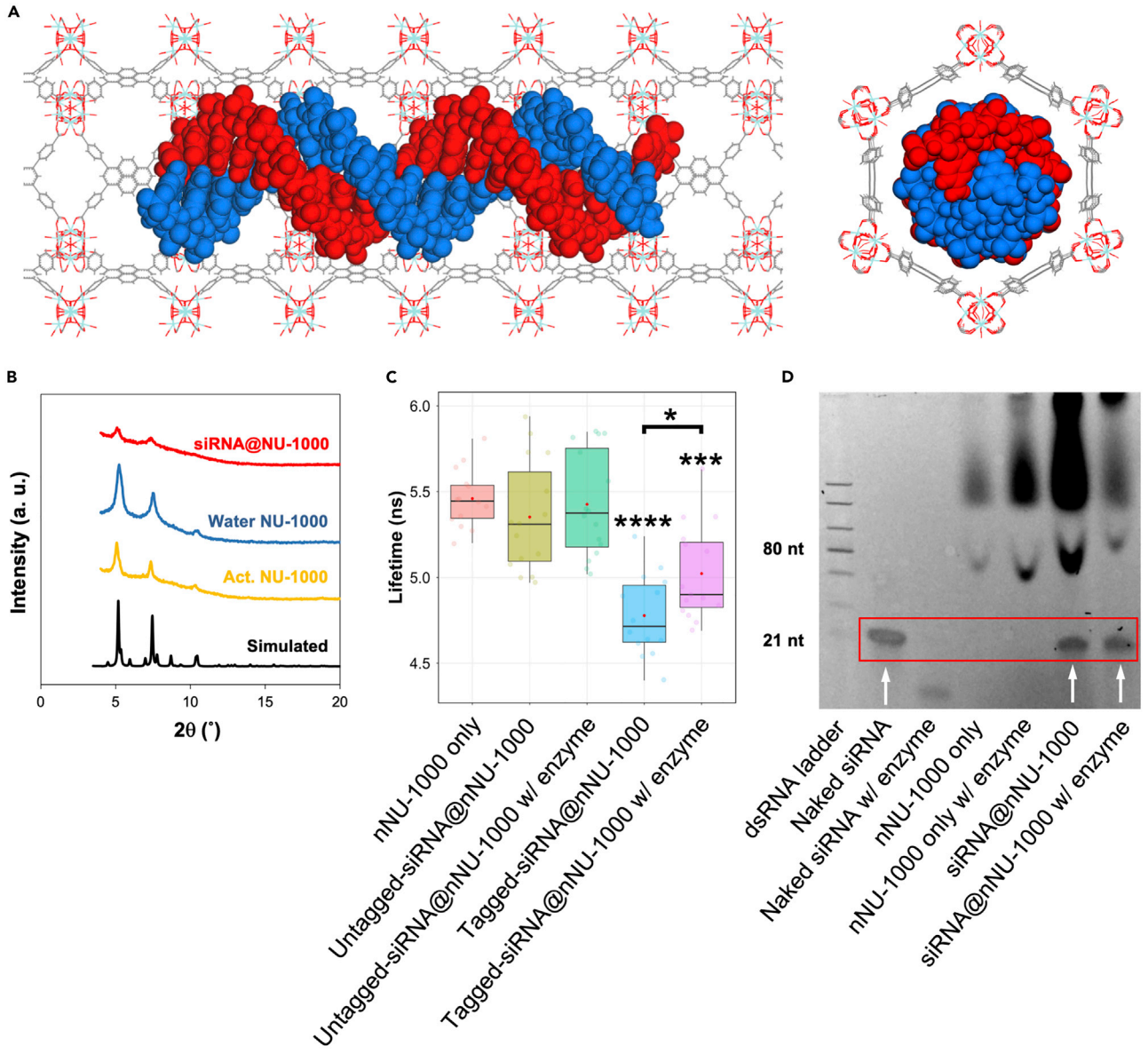

Figure 2. Encapsulation of siRNAs with NU-1000

(A) Schematic lateral and top view of a section of the NU-1000 pore channel with one double-stranded siRNA molecule (red and blue intertwined space filling structure).

(B) Powder X-ray diffraction (PXRD) patterns of simulated NU-1000, activated nNU-1000, nNU-1000 soaked in water, and siRNA-loaded nNU-1000.

(C) Fluorescence-lifetime imaging microscopy (FLIM) analysis of different systems. Data are shown in box-and-whiskers style, where "box" represents 1st quartile, median, and 3rd quartile, and "whiskers" (lines) represent minimum and maximum values. Averages are represented by the red dots. Individual data points are shown in faint colored circles with outliers as gray circles. 15 lifetime images were acquired per condition. Statistical analysis was carried out using one-way ANOVA followed by Sidak's Multiple Comparisons test (****$p < 0.0001$, ***$p < 0.001$, *$p < 0.05$).

(D) 20% TBE polyacrylamide gel stained with PAGE GelGreen for the enzyme degradation protection analysis of different systems. A dsRNA ladder on far right of gel gives location of 21-nt length fragments. White arrows indicate the presence of non-degraded siRNAs.

We then loaded siRNAs into the MOF nanoparticles—nNU-1000. Figure 2B shows the powder X-ray diffraction (PXRD) patterns of nNU-1000 and loaded samples and the comparison with the simulated pattern. The nNU-1000 was activated at 100°C for 3 days to ensure that all potential solvent inside the pore structure was removed. The main peaks are preserved, but some minor ones are lost when compared with the calculated pattern; this is compatible with the small particle

Please cite this article in press as: Teplensky et al., A Highly Porous Metal-Organic Framework System to Deliver Payloads for Gene Knockdown, Chem (2019), https://doi.org/10.1016/j.chempr.2019.08.015

size of nNU-1000. We then soaked nNU-1000 in RNAse-free water at the same MOF concentration as our siRNA-loaded sample (20 mg/mL) and observed excellent agreement with the PXRD pattern of the activated nNU-1000. However, the loading of siRNAs in nNU-1000 (siRNA@nNU-1000) led to a decrease in the intensity of the major peaks. This is consistent with a notion that the siRNAs are adsorbed inside the porous MOF cavity, causing a decrease in the contrast between phases (i.e., the framework and the empty or filled porosity) and therefore a decrease of the peak intensity. The amount of siRNA loaded, measured from the liquid supernatant, was approximately 150 pmol/mg of nNU-1000, as quantified by an RNA-specific fluorescence marker.

As mentioned above, enzymatic degradation is one of the major drawbacks in siRNA therapy. The question of whether the siRNAs are located inside the MOF's porosity or outside on the external surface—or in both locations—is therefore critical for its efficient transfection. We first evaluated the localization of the siRNA through fluorescence-lifetime imaging microscopy (FLIM). The fluorescence lifetime is sensitive to the micro-environment of a fluorescent molecule[44] and can provide an indirect readout on intermolecular interactions on the scale of a few nanometers. We used time-correlated single photon counting (TSCPC) to quantify FLIM signals. Loading MOFs with fluorescently labeled siRNAs results in a drop in the lifetime of the intrinsic fluorescence emission from the MOF material because of energy transfer from the MOF scaffold to the dye. We loaded nNU-1000 with a high concentration of siRNAs, using both tagged and non-tagged varieties. We then reacted these samples with an enzyme that can cleave siRNA of 21 nt in length. Since the enzyme is too large to enter into the porous MOF structure, it will be able to degrade only the siRNAs that are exposed on the external surface of the MOF. Figure 2C shows the fluorescence lifetimes for five experimental conditions: nNU-1000 only; siRNA-, untagged or tagged, loaded nNU-1000; and enzyme-reacted-siRNA-, untagged or tagged, loaded nNU-1000. The fluorescence lifetime for the MOF alone is 5,497 $\pm$ 60 ps. This value decreases slightly but not significantly to 5,352 $\pm$ 80 ps for the untagged-siRNA@nNU-1000, indicating that without the fluorophore, there is no energy transfer and therefore no effect on the MOF's fluorescence lifetime. The enzyme reacted with the untagged-siRNA@nNU-1000 also shows a negligible change in lifetime (5,492 $\pm$ 80 ps). However, the lifetime of the tagged-siRNA@nNU-1000 drops significantly ($p < 0.0001$) to 4,718 $\pm$ 80 ps, indicating that the MOF fluorescence is quenched due to a fluorescence resonance energy transfer (FRET)-like process between the labeled siRNA and the MOF scaffold that it occupies. In the case of the enzyme-reacted tagged-siRNA@nNU-1000, we observed a statistically significant increase ($p < 0.05$) up to 5,023 $\pm$ 70 ps. This noticeable increase in lifetime from the non-enzyme-reacted to the enzyme-reacted structure of ca. 300 ps suggests that some level of siRNA degradation is occurring. In order for the enzyme to degrade the siRNA, some siRNAs must be located externally on the MOF's surface. However, the more prominent decrease in the lifetime of ca. 500 ps between the nNU-1000 only and the tagged-siRNA@nNU-1000 with enzyme ($p < 0.001$) suggests that the majority of the siRNAs are loaded in the internal porosity of nNU-1000.

To further analyze the capacity of nNU-1000 to protect siRNA, we designed an enzyme protection assay. Figure 2D shows the presence of the siRNA, measured on a gel, after exposure to the enzyme described above. As a control, we observed that the 21-nt band in the gel for the naked, unprotected siRNA disappears when exposed to the enzyme, confirming that this enzyme cleaves siRNA sequences of this length. We also verified that nNU-1000 would not show a false positive band

Please cite this article in press as: Teplensky et al., A Highly Porous Metal-Organic Framework System to Deliver Payloads for Gene Knockdown, Chem (2019), https://doi.org/10.1016/j.chempr.2019.08.015

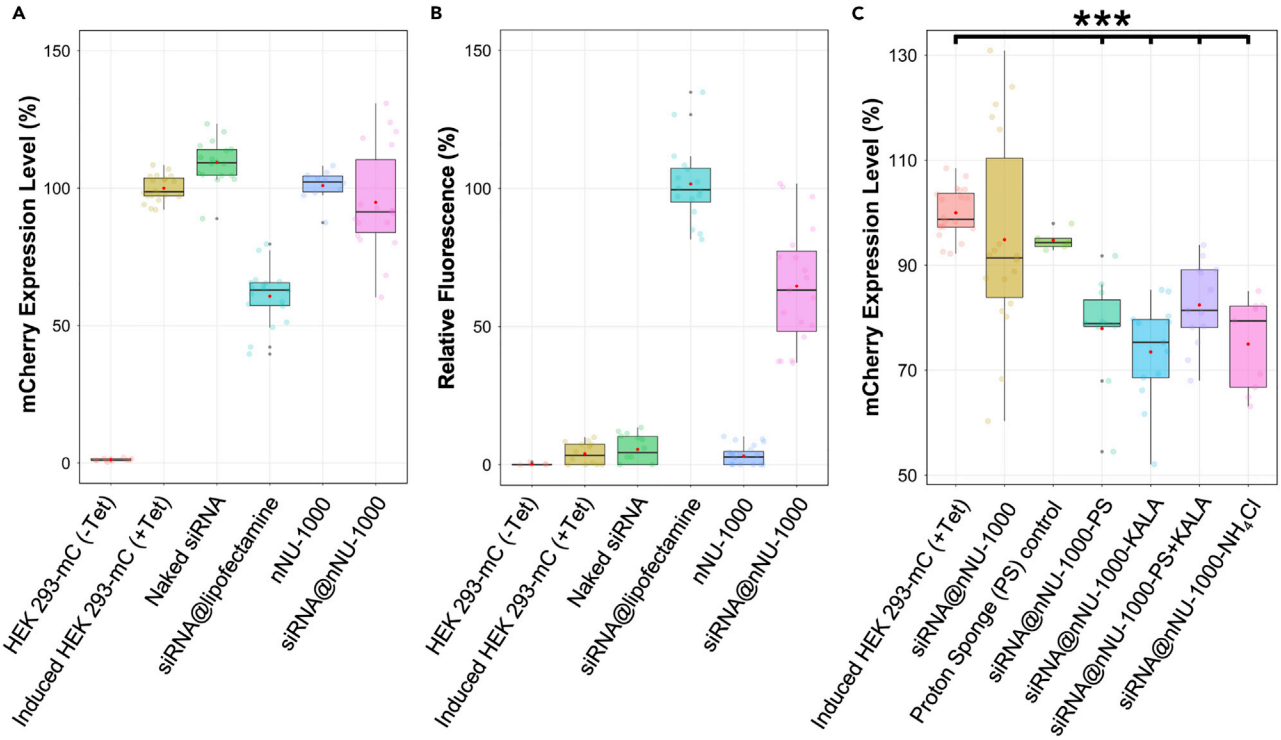

Figure 3. *In Vitro* Performance of siRNAs Loaded in NU-1000

(A) mCherry expression level in HEK293-mC cells as quantified by flow cytometry after 24 h incubation.

(B) Alexa Fluor 647 fluorescence of siRNA tagged, as quantified by flow cytometry and normalized to positive control, siRNA@lipofectamine.

(C) Comparison of mCherry expression level in HEK293-mC cells when using different cofactors. Plots are shown in box-and-whiskers style, where "box" represents 1st quartile, median, and 3rd quartile, and "whiskers" (lines) represent minimum and maximum values; averages are represented by the red dots. Individual data points are shown in faint colored circles with outliers as gray circles. Each condition was run with a minimum of 9 replicates with some conditions having up to 24 replicates. Statistical significance was calculated through one-way analysis of variance (one-way ANOVA) and a post-Dunnett's Multiple Comparison Test compared to the induced HEK293-mC (+Tet) (*** $p < 0.001$).

on the gel at the 21-nt siRNA location; most of the MOF residue remaining post-purification gets trapped higher up on the gel, with bright and smeared bands at around 80 nt and above, as marked by the ladder. In addition, there is no change in the gel pattern for nNU-1000 reacted with the enzyme, demonstrating that the enzyme would not cleave any MOF components to a similar size as the 21-nt band. After purification of the siRNAs from the siRNA@nNU-1000 sample, both with and without exposure to the enzyme, bands are present at the 21-nt location, demonstrating the capability of nNU-1000 to protect the siRNAs from enzymatic degradation.

In Vitro Effect of siRNA on mCherry Cell Line

With the characterized siRNA@MOF system, we aimed to quantify the signal knockdown and efficacy *in vitro*. We activated the inducible HEK293-mC cell line with tetracycline and incubated it with various controls along with the siRNA@NU-1000. Figure 3A shows the results of the mCherry expression levels normalized to induced HEK293-mC cells; Table 1 highlights the first quartile, median, third quartile, and interquartile range (IQR) values for the different experiments. We can first confirm that these cells do not express mCherry when not induced—in this case, expression levels are around 1.2%. This figure also demonstrates the ineffectiveness of the naked siRNAs when added to the cells, as mCherry expression levels did not deviate significantly from those of untreated induced cells. The positive control,

Please cite this article in press as: Teplensky et al., A Highly Porous Metal-Organic Framework System to Deliver Payloads for Gene Knockdown, Chem (2019), https://doi.org/10.1016/j.chempr.2019.08.015

Table 1. *In Vitro* Performance of siRNAs Loaded in NU-1000

mCherry Expression Levels	Non-induced	Tetracycline Induced	Naked siRNA	siRNA@ lipofectamine	nNU-1000	siRNA@ nNU-1000	Proton Sponge (PS)	siRNA@ nNU-1000 -PS	siRNA@ nNU-1000 -KALA	siRNA@ nNU-1000 -PS+KALA	siRNA@ nNU-1000 -NH_4Cl
Q1	1	97.2	104.7	57.3	98.7	83.9	93.6	78.3	68.6	78.1	66.8
Median	1.1	98.7	109.3	63	102.3	91.4	94.3	78.9	75.3	81.4	79.4
Q3	1.6	103.7	114.1	65.6	104.4	110.4	95.1	83.4	79.7	89.1	82.2
IQR	0.6	6.5	9.4	8.3	5.7	26.5	1.6	5.1	11.1	11	15.4

Comparison between 1st quartile (Q1), 3rd quartile (Q3), and the interquartile range (IQR) for the normalized mCherry expression level in HEK293-mC cells as quantified by flow cytometry. Each condition was run with a minimum of 9 replicates with some conditions having up to 24 replicates.

siRNA@lipofectamine, shows a significant decrease of 40% in signal compared to the normalized signal from induced HEK293-mC cells. We also verified that the nNU-1000 did not by itself affect cellular expression levels of mCherry, as the mean value stays near 100%. Interestingly, when we added the siRNA@nNU-1000 complex, we observed a wide range of results. At times, there was no change in the mCherry expression, and at other times, the mCherry expression would be nearly as low as the positive control siRNA@lipofectamine. In other words, whereas the IQR (i.e., the box height) values for the previous cases was rather low, in the range of 5.7 and 9.4, it significantly increased for siRNA@NU-1000 up to 26.5 (i.e., 219% increment compared to siRNA@lipofectamine). To understand this increase in the variability of mCherry expression levels, we utilized a siRNA tagged with a fluorophore at 647 nm to assess the internalization of the siRNA@nNU-1000 complex in the HEK293-mC cells. Figure 3B shows the fluorescence of Alexa Fluor 647, representing the quantity of siRNAs, normalized to the positive control. As expected, we found minimal fluorescence in normal non-induced cells and induced cells, both without the addition of siRNAs. The observed signal is attributed to auto-fluorescence with no statistical difference between normal non-induced cells, induced cells, cells with naked siRNA added or cells with nNU-1000 only added. This confirms that no siRNA is present inside any of the cells. siRNA@nNU-1000 was taken up into cells nearly as efficiently as siRNA@lipofectamine but was not as effective at knocking down mCherry expression. Since siRNA must be in the cytoplasm to be effective in its signal knockdown pathway, we hypothesized that the inconsistent and variable levels of mCherry gene knockdown are caused by siRNA@NU-1000 complex entrapment and degradation in endosomes, and that siRNA consequently gets degraded before it is released in the cytoplasm.

To test the hypothesis of siRNA@NU-1000 entrapment in endosomes, we added to the siRNA@nNU-1000 complex various factors including proton sponges or membrane opening peptides that are able to either break or open endosomes.[24,45,46] We used Proton-Sponge (PS), the amphipathic KALA peptide, and ammonium chloride (NH_4Cl). First, we used FLIM on an Oregon Green-488-conjugated dextran—with the size that can enter through clathrin-mediated endocytosis, comparable to the pathway of entry that our nNU-1000 MOF uses—to quantify the capability of these endosomal release factors to avoid endosomal entrapment. Fluorescence lifetime increased significantly with pH (Figure S3), These results suggest that the cofactors PS and NH_4Cl are acting in a mechanism that is increasing the vesicular pH from its normal value, whereas KALA, on the contrary, a cell-penetrating peptide is not explicitly acting as a proton absorber. Figure 3C shows the results of the mCherry expression levels for these complexed systems compared to the untreated induced HEK293-mC cells. We incubated the siRNA@nNU-1000 with either 0.04 mg of the PS cofactor (~2.7 wt % of the complex if 100% loaded), 0.4 μg of the KALA cell-penetrating peptide, or 0.1 μmol (or 5.3 μg) of ammonium chloride. We believe that the

Please cite this article in press as: Teplensky et al., A Highly Porous Metal-Organic Framework System to Deliver Payloads for Gene Knockdown, Chem (2019), https://doi.org/10.1016/j.chempr.2019.08.015

small cofactors can be on both the external surface and in the internal porosity, whereas KALA is on the external surface due to its large size. The use and incorporation of a cell-penetrating or targeting peptide and complexation of endosomal release cofactors to our siRNA@MOF system is an element of novelty for this study. When the PS was added (siRNA@nNU-1000-PS), the average expression decreased to ca. 78% of the normal induced HEK293-mC cells. Compared to the impact on mCherry expression of the PS or the nNU-1000 alone, with expression values of ca. 95% and 100%, respectively, this decrease is statistically significant ($p < 0.01$ and $p < 0.001$, respectively). When using KALA (siRNA@nNU-1000-KALA), we observed a decrease in mCherry signal to ca. 73%. Interestingly, when we co-loaded the MOF with both of these compounds (siRNA@nNU-1000-PS+KALA), we observed a reduction to ca. 82%, a value that is not statistically different from those of siRNA@nNU-1000-PS and siRNA@nNU-1000-KALA. While literature suggested different mechanisms of action for these particular two cofactors, it was not known if there would be a more efficient response if both were included together. Our results indicate that there is not a cumulative effect of the two compounds. When we added a different compound, ammonium chloride, to the siRNA@MOF complex (siRNA@nNU-1000-NH_4Cl), we observed mCherry expression at ca. 75% of the induced HEK293-mC cell value. Regardless of the specific cofactor, when complexed together with the siRNA@nNU-1000, they assisted in the gene knockdown capabilities of the system. The relatively high mCherry expression levels for all the systems, including lipofectamine positive control, with knockdown levels below 50%, could be related to the long half-life of the protein. Importantly, we were able to reach, in some cases, knockdown effects on par with that of the positive control siRNA@lipofectamine.

Super-resolution Microscopy Analysis of *In Vitro* Trends

We performed experiments *in vitro* using structured illumination microscopy (SIM)[31,47] to get a visual picture of the uptake and release processes discussed. Figure 4 shows 3-color images of HEK293-mC cells where we have labeled the early endosomes with an RFP marker. In addition, we incubated the cells with either naked Alexa-Fluor-647-tagged siRNA (Figure 4A), Alexa-Fluor-647-tagged siRNA@lipofectamine, the same positive control we used in the previous experiment (Figure 4B); siRNA@nNU-1000 (Figure 4C) and siRNA@nNU-1000-KALA (Figure 4D). In all images, the tagged siRNAs can be visualized in red; the nNU-1000, when present, is colored in green; and the early endosomes are shown in blue. We chose to stain the early endosomes as opposed to other cellular organelles in an attempt to visualize the point at which the siRNA@nNU-1000 complex dissociates from the endosome, as it must do this to effectively deliver the siRNA into the cytoplasm. As determined previously,[31] nNU-1000 requires active transport to enter cells. It was thus expected that the systems with MOF would colocalize with the early endosomes, whereas the naked siRNA and the siRNA@lipofectamine would not. In agreement with our observations from flow cytometry, we observe that little, if any, of the tagged siRNA signal is located intracellularly (Figure 4A). When using siRNA@lipofectamine, we observed a large amount of tagged siRNA intracellularly—but not colocalized with the endosome (Figure 4B). The lack of endosome colocalization is portrayed with the distinctive red marks in the cell. In the case of siRNA@nNU-1000, the complex directly overlaps with early endosomes, shown by white color indicative of 3-color overlap (Figure 4C). Two specific instances of 3-color overlap are pointed out by the white arrows, indicating that both the siRNA and nNU-1000 are contained within a vesicle—meaning the siRNA would be unable to act with the RISC complex in the cytosol and gene knockdown would not occur. In the case of siRNA@nNU-1000-KALA, the white arrow highlights a position of 2-color

Please cite this article in press as: Teplensky et al., A Highly Porous Metal-Organic Framework System to Deliver Payloads for Gene Knockdown, Chem (2019), https://doi.org/10.1016/j.chempr.2019.08.015

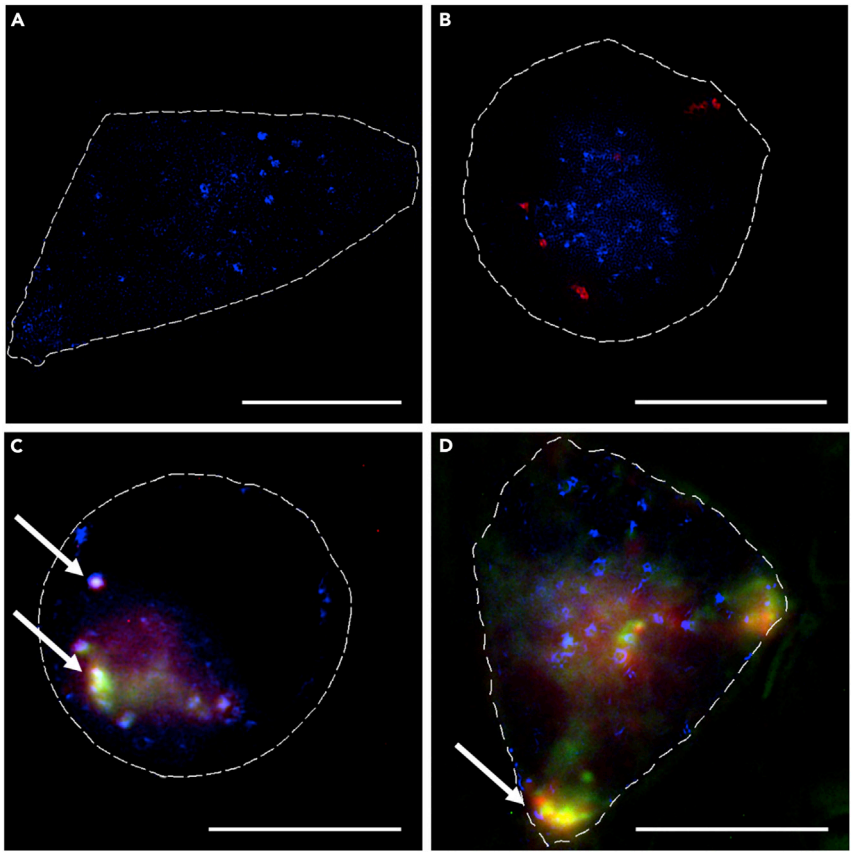

Figure 4. Representative SIM Images of siRNA Uptake into HEK293-mC Cells

Images of HEK293-mC Cells Incubated with (A) naked Alexa-Fluor-647-tagged siRNA, (B) Alexa-Fluor-647-tagged siRNA@lipofectamine, (C) Alexa-Fluor-647-tagged siRNA@nNU-1000, and (D) Alexa-Fluor-647-tagged siRNA@nNU-1000 KALA. Early endosomes stained in blue; Alexa-Fluor-647-tagged siRNA in red; nNU-1000 in green. Blue channel taken with SIM; red and green channels taken in wide field. Cell outlines are shown by dashed white lines. Scale bars, 10 μm. The arrows indicate instances of 2- or 3-color overlap.

overlap between the siRNA and nNU-1000, shown by the yellow color instead of white (Figure 4D). This demonstrates an example of an siRNA not trapped within an endosome and able to bind with the RISC complex and initiate the RNAi pathway. The lack of white color (i.e., the 3-color overlap) in Figure 4D supports our hypothesis about the endosomal release factors helping the siRNA@nNU-1000 to evade endosomal retention, and also is a representative example image of the trends we noted in Figure 3.

Conclusions

In this study, we demonstrate the successful development and proof-of-concept efficacy of a Zr-based MOF, nNU-1000, that is able to load, protect, and deliver siRNA effectively in the cytoplasm to knockdown gene expression. We performed molecular simulations to select the MOF that favored internalization of the siRNA. We characterized the loading of the siRNAs into the MOF by PXRD, where the broadening, decreased intensity, and elimination of some peaks indicated that the siRNAs interacted with the framework in a way that decreased the contrast of the peak intensity, as well as reduced the crystallinity. An enzyme degradation stability study demonstrated that the siRNAs were protected by the MOF, as relevant 21-nt bands were

Please cite this article in press as: Teplensky et al., A Highly Porous Metal-Organic Framework System to Deliver Payloads for Gene Knockdown, Chem (2019), https://doi.org/10.1016/j.chempr.2019.08.015

still observed on a polyacrylamide gel after an enzymatic attack. We performed studies to elucidate the location of the siRNAs within or on the framework using FLIM. These results suggest that a negligible amount of siRNAs were located external to the MOF's surface; thus, the majority of the siRNAs were loaded within the internal porosity of the structure. *In vitro* studies at first suggested that the siRNA was able to enter the cell when carried by nNU-1000, but that efficacy was inconsistent. Based on the hypothesis that this was due to endosomal entrapment, we complexed the siRNA@MOF system with various factors—species that are able to open up endosomes through various mechanisms. By taking advantage of these factors, it was possible to observe consistent levels of knockdown. SIM images show representative examples of the trends that we noted in the flow cytometry and indicate instances along the endosomal uptake pathway at which the siRNA@MOF complex is able to separate from the early endosomes. To the best of our knowledge, this work is the first to utilize a large porous network to internally encapsulate siRNAs in sufficient quantities to achieve gene knockdown—150 pmol/mg MOF. The stability of the MOF material offers future advantages in long-term storage, while the tunability of the MOFs can allow further modifications to improve efficacy. Through this work, we show how the efficacy and efficiency of gene therapy can be improved with the implementation of this highly porous material.

EXPERIMENTAL PROCEDURES

Materials

NU-1000 (also referred to as nNU-1000, 150 nm size) was obtained via synthesis published in previous protocols.[48] Custom siRNA (sense strand 5′-AAGGAGTTCAT GCGCTTCAAG-3′) and custom-tagged siRNA (sense strand 5′ Alexa Fluor 647 tag) were ordered from Eurogentec. HEK293 T-rex Flp-In cells were obtained from the ATCC and were modified with a T-REx insert as published in the literature.[40] They were cultured with Dulbecco's modified Eagle's medium (DMEM, Sigma-Aldrich D5671), fetal bovine serum (FBS, Sigma-Aldrich F9665), 100× 200 mM L- glutamine (Life Technologies 25030024), penicillin and streptomycin (P-S, Life Technologies 15140122), hygromycin (Thermo Fisher, 10687010, 100 μg/mL final concentration), and blasticidin (Thermo Fisher, R21001, 15 μg/mL final concentration). PBS (Sigma D8537) and 1× trypsin-EDTA (Life Technologies 25300054) were used. Trypan blue was purchased from Thermo Fisher (UK, 15250061). Opti-MEM Reduced Serum Medium GlutaMAX Supplement and Lipofectamine RNAiMAX Transfection Reagent were purchased from Thermo Fisher (51985034 and 13778030, respectively). All enzymes and gel ladders used were purchased from New England Biolabs. Novex 20% TBE polyacrylamide gel (EC63155BOX) and Hi-Density TBE Sample Buffer (LC6678, 5×) were bought from Thermo Fisher. A PAGE GelGreen Nucleic Acid stain was purchased from Biotium and the Zymo Oligo Clean & Concentrator kit was obtained from Cambridge Bioscience (UK, D4061). A Qubit microRNA Assay Kit was used (Thermo Fisher Q32880). Stains for endosomes were obtained from ThermoFisher (CellLight Early Endosomes-RFP BacMam 2.0, C10587). PS (99%) was obtained from Sigma-Aldrich (158496) and the KALA peptide, from AnaSpec (AS-65459). All chemicals and biochemicals used were of analytical grade.

Molecular Mechanics Modeling

A simplified model of the siRNA and nNU-1000 system was constructed in the Materials Studio software package[49] and was created from the NU-1000 crystallographic data published previously.[38] It consists of ten hexagonal rings of Zr-oxide nodes, extended ca. 160 Å along the channel. A number of structures were considered, each with different arrangements of the siRNA molecule inside the hexagonal channel of NU-1000. Bonded and non-bonded interactions between all framework

Please cite this article in press as: Teplensky et al., A Highly Porous Metal-Organic Framework System to Deliver Payloads for Gene Knockdown, Chem (2019), https://doi.org/10.1016/j.chempr.2019.08.015

atoms were described by the Universal Force Field (UFF),[50] and the structures were optimized using the Forcite module in Materials Studio, using an algorithm that is a cascade of the steepest descent, adjusted basis set Newton-Raphson and quasi-Newton methods. To estimate the energy associated with the siRNA molecule in NU-1000, we calculated the total energy of the hexagonal channel containing the siRNA molecule ($E_{channel+siRNA}$) and subtracted the energies obtained from the isolated channel ($E_{channel}$) and siRNA molecule (E_{siRNA}) according to: $E_{ads} = E_{channel+siRNA} - E_{channel} - E_{siRNA}$.

X-Ray Diffraction

Room temperature PXRD was performed on nNU-1000 loaded and unloaded samples using a Bruker-D8 theta/theta machine with CuKα1 (λ = 1.5405 Å) radiation and a LynxEye position sensitive detector in Bragg Brentano parafocusing geometry. Steps were performed for 2θ = 2° to 50°.

siRNA Adsorption and Subsequent Cofactor Addition

Samples of nNU-1000 were measured (1.5 mg each), and mCherry-encoding siRNA was added in a ratio of 1:2—tagged siRNA:untagged siRNA—for a total of 15 μL of 10 μM siRNA. The tag was an Alexa Fluor 647 on the 5′ end of the sense strand. RNase-free water was added to each such that the final concentration of MOF was 20 mg/mL, and all samples were incubated at 37°C for approximately 2.5 h. Some samples then had a subsequent cofactor addition. For PS, the calculation was as follows: the amount of metal cluster sites in the MOF sample, in mol, was determined (approximated to one-third the mol of MOF calculated). Half of this molar amount of cluster sites was converted to g of PS. A solution of PS was then created such that 10 μL of this PS solution was added to the respective sample. For KALA, 10 μL of a 0.04 mg/mL solution in RNAse-free water was added to the respective sample. For ammonium chloride, 10 μL of a 10 mM solution in RNAse-free water was added to the sample. All samples were incubated for another hour at 37°C. After the 1 h incubation, the samples were centrifuged at 14,000 rpm for 60 s, and the supernatant was removed.

siRNA Qubit Quantification

To quantify the amount of siRNAs in a supernatant solution, we used the Qubit microRNA Assay Kit (ThermoFisher Q32880). All samples were purified with the Zymo Oligo Clean & Concentrator kit prior to incubation with the Qubit Assay kit and measured with the Qubit Fluorimeter. 10 μL aliquot of each purified sample was used.

siRNA Enzyme Degradation Stability Analysis

5 mg of nNU-1000 were incubated with 75 μL of 10 μM untagged siRNA. RNAse-free water was added to the mixture such that the final concentration of MOF was 20 mg/mL. Negative controls of naked siRNA and negative controls of MOF only, each with and without enzyme, were also prepared with the same concentration and relative amounts of siRNA and nNU-1000, respectively. The mixture was placed in a 37°C incubator for approximately 2.5 h. The samples containing MOF were centrifuged at 14,000 rpm for 60 s, and the supernatant was removed. For those samples that were acting as a negative control for enzyme, 10 μL of NEB Buffer 2 (10×) and 82.5 μL of RNAse-free water were added to the samples. For the conditions testing enzyme protection, 10 μL of NEB Buffer 2 (10×), 72.5 μL of RNAse-free water, and 10 μL of Shortcut RNAse III enzyme were added. All samples were mixed and incubated for 20 min at 37°C before the addition of 10 μL of 10× EDTA. In order to release the siRNAs from the MOF to run on a gel, 100 μL of

Please cite this article in press as: Teplensky et al., A Highly Porous Metal-Organic Framework System to Deliver Payloads for Gene Knockdown, Chem (2019), https://doi.org/10.1016/j.chempr.2019.08.015

10× PBS was added to each sample, and the samples were vortexed until dispersed. Using a Zymo Oligo Clean & Concentrator kit, the samples were all purified to remove residue MOF or linker. A Novex 20% TBE polyacrylamide gel was loaded using 8 μL of the purified product of each sample and 2 μL of Hi-Density TBE Sample Buffer (5×). A dsRNA ladder (NEB #N0363S) was also run. The gel was run at 200 V for 45 min, after which it was soaked in 100 mL of dH_2O with 10 uL of PAGE GelGreen (Biotium) for approximately 1.5 h. It was imaged using a Syngene G:Box.

siRNA Location Analysis Prep for Fluorescence-Lifetime Imaging Microscopy

Samples of nNU-1000 (ca. 0.2 mg) were incubated at 37°C for 2.5 h with either 100 μL of nuclease-free water, as a negative control, or 100 μL of 100 μM tagged siRNA. After loading, the samples were centrifuged at 14,000 rpm for 90 s, the supernatant was removed and used to measure a background, and 200 μL of DMEM without phenol red was added to each of the samples. For the enzyme-reacted sample, 100 μL of the sample loaded with tagged siRNA was spun down again at 14,000 rpm for 60 s. The supernatant was removed and 10 μL of Shortcut RNAse III enzyme was added along with 72.5 μL of RNAse-free water, and 10 μL of NEB Buffer 2 (10×). This was incubated for 20 min at 37°C before the addition of 10 μL of 10× EDTA. This entire sample was then spun down again at 14,000 rpm for 60 s, after which the supernatant was removed, and 200 μL of DMEM without phenol red was added to the sample.

Fluorescence-Lifetime Imaging Microscopy

All samples were assayed on a home-built, confocal-based FLIM platform using time-correlated single photon counting (TCSPC). The equipment is a modified version of a published multiparametric imaging system[51] and equipped with a 100× objective lens (UPLS Apo, 100× oil, 1.4NA, Olympus, Germany). A pulsed supercontinuum source (WL-SC-400-15, Fianium Ltd., UK, pulse width 6ps, repetition rate 40 MHz) was used for excitation in conjunction with a tuneable filter (AOTFnC-400.650, Quanta Tech, New York, USA), an excitation filter FF01-474/27, and an emission filter FF01-542/27 (both from Semrock Inc., New York, USA). Photons were recorded in a time-tagged, time-resolved mode that permits sorting photons from each pixel into a histogram according to the arrival times after the last laser pulse. The laser intensity at the samples was 60 μW. The data were recorded by SPC-830 (Becker and Hickl GmBH, Germany). Photons were acquired for 2 min to make a single 256× 256 FLIM image. The TCSPC histograms for each pixel were fitted with a double exponential decay function using FLIMfit.[52] The longer lifetime component τ_2 of the MOF fluorescence decay varied between different conditions and was plotted. Statistical analysis was carried out using one-way ANOVA followed by Dunnett's multiple comparisons test in Graphpad Prism software (La Jolla, California, USA).

Structured Illumination Microscopy Imaging

HEK293-mC cells were cultured before being seeded at a density of 75,000 cell/mL and 0.4 mL per well on an 8-well LabTek Dish (Thermo Fisher 155409) for 1 day. Cells were then incubated with 1.875 μL per well of BacMam Early Endosome Stain overnight. The following day, the entire well contents were removed, and the cells were incubated with the different conditions for MOF prepared following the same protocol described in siRNA Adsorption and Subsequent Cofactor Addition, above. The cells were incubated with these different conditions for 4 h. Post-incubation, media were removed from each well, washed once with 1× PBS, and replaced with non-phenol red complete DMEM for SIM Imaging. Images of the samples were collected using a custom-built 3-color structured illumination microscopy (SIM) setup which we

have previously described.[53] A60×/1.2NA water immersion lens (UPLSAPO 60XW, Olympus) focused the structured illumination pattern onto the sample. This lens also captured the samples' fluorescence emission light before imaging onto an sCMOS camera (C11440, Hamamatsu). Laser excitation wavelengths used were 488 nm (iBEAM-SMART-488, Toptica), 561 nm (OBIS 561, Coherent), and 640 nm (MLD 640, Cobolt), to excite the fluorescence emission of MOF, early endosomes, and siRNA-tag, respectively. The laser intensity at the samples was between 10 and 20 W/cm^2. Upon reconstruction, it was found that the intensity of the signal of the MOF and siRNA was too low for artifact-free SIM reconstruction, so widefield reconstruction was used in these channels. SIM reconstruction for the endosome channel was performed in fairSIM,[54] to utilize the latest developments in open-source SIM reconstruction.

siRNA Efficacy Analysis

HEK293 T-REx Flp-In cells with an inducible mCherry protein, referred to as HEK293-mC cells, were cultured before being seeded at a density of 140,000 cell/mL with 1 mL per well on a 12-well Nunc Dish (ThermoFisher 150628) for approximately 24 h. The cells were activated with tetracycline (final concentration: 1 μg/mL) and incubated overnight. While the cells were incubating, different conditions for MOF were prepared as described in siRNA Adsorption and Subsequent Cofactor Addition, above. 1 mL of complete DMEM media was added to each sample. The samples were sonicated for ca. 1 min. 200 μL of this solution was added to the respective wells. For the non-MOF conditions (naked siRNA and siRNA@lipofectamine), 1 mL of complete DMEM media was added to each well prior to adding the following. For the naked-siRNA condition, 3 μL of 10 μM siRNA in a 1:2 ratio—tagged siRNA:untagged siRNA—was added to each well. For the siRNA@lipofectamine condition, 50 μL of Opti-MEM Reduced Serum Medium GlutaMAX Supplement was mixed with 3 μL lipofectamine in one tube, and 6 μL of 10 μM siRNA in a 1:2 ratio—tagged siRNA:untagged siRNA—in another tube. 50 μL of each solution was then combined and pipetted briefly before being incubated at room temperature for 5 min. After 5 min, 50 μL of this solution was added to each well. All conditions were left to incubate for 24 h. Post-condition incubation, the media was removed from each well; washed once with 1× PBS, once with trypan blue, and twice more with 1× PBS; and then incubated for 5 min at 37°C with trypsin. Fresh complete DMEM without phenol red was added to the wells after trypsin incubation, and the entire contents were transferred to Eppendorf tubes and centrifuged at 1,200 rpm for 5 min. The cells were resuspended in 500 μL of complete DMEM without phenol red. Samples were measured immediately on a Cytek DxP8 analyzer cytometer. The analysis was completed with FlowJo software (Becton, Dickinson & Company subsidiary) and Graphpad Prism software (La Jolla, California, USA).

SUPPLEMENTAL INFORMATION

Supplemental Information can be found online at https://doi.org/10.1016/j.chempr.2019.08.015.

ACKNOWLEDGMENTS

This project has received funding from the European Research Council (ERC) under the European Union's Horizon 2020 research and innovation programme (NanoMOFdeli), ERC-2016-COG 726380, and (SUPUVIR) no. 722380. M.H.T. thanks the Gates Cambridge Trust for funding, S. Haddad for helpful discussions, and A. Li for assistance with data visualization. D.F.-J. thanks the Royal Society for funding through a University Research Fellowship. S.B.d.Q.F., F.M.R., and D.I.J. were funded

by Cancer Research UK Senior Group Leader Grant CRUK/A15678. O.K.F. gratefully acknowledges DTRA for financial support (grant HDTRA-1-14-1-0014). C.F.K. acknowledges funding from the UK Engineering and Physical Sciences Research Council (grants EP/L015889/1 and EP/H018301/1), the Wellcome Trust (grants 3-3249/Z/16/Z and 089703/Z/09/Z) and the UK Medical Research Council (grants MR/K015850/1 and MR/K02292X/1), and Infinitus (China) Ltd. Computational work was supported by the Cambridge High Performance Computing Cluster, Darwin.

AUTHOR CONTRIBUTIONS

Conceptualization, M.H.T. and D.F.-J.; Methodology, M.H.T. and D.F.-J.; Investigation, M.H.T., M.F., C.P., C.H., M.L., A.G., and P.L.; Software, M.A.-A. and P.Z.M.; Writing – Original Draft, M.H.T. and D.F.-J.; Writing – Review & Editing, M.H.T., M.F., C.P., C.H., M.L., A.G., M.A.-A., P.Z.M., P.L., O.K.F., S.B.d.Q.F., F.M.R., D.I.J., G.K.S., C.F.K., and D.F.-J.; Supervision, O.K.F., S.B.d.Q.F., F.M.R., D.I.J., G.K.S., C.F.K., and D.F.-J.; Project Administration and Funding Acquisition, D.F.-J.

DECLARATION OF INTERESTS

D.F.-J. is a founder of Immaterial Labs and a member of its scientific advisory board; P.Z.M. is a consultant for Immaterial Labs. O.K.F. is a founder of NuMat and a member of its scientific advisory board. All the other authors declare no other competing interests. M.H.T., C.H., G.K.S., and D.F.-J. have filed a patent related to this work.

Received: April 26, 2019
Revised: June 11, 2019
Accepted: August 21, 2019
Published: September 16, 2019

REFERENCES AND NOTES

1. Smith, E. (2016). Tackling hard-to-treat cancers – what, how and why?. http://scienceblog.cancerresearchuk.org/2016/07/20/tackling-hard-to-treat-cancers-what-how-and-why/.

2. Cancer Research UK Cancer survival for common cancers. http://www.cancerresearchuk.org/health-professional/cancer-statistics/survival/common-cancers-compared#heading-Zero.

3. National Cancer Institute (2017). Types of cancer treatment. https://www.cancer.gov/about-cancer/treatment/types.

4. Miller, K.D., Siegel, R.L., Lin, C.C., Mariotto, A.B., Kramer, J.L., Rowland, J.H., Stein, K.D., Alteri, R., and Jemal, A. (2016). Cancer treatment and survivorship statistics, 2016. CA Cancer J. Clin. *66*, 271–289.

5. American Cancer Society (2019). Cancer Facts & Figures 2019 (American Cancer Society).

6. A.M. Noone, N. Howlader, M. Krapcho, D. Miller, A. Brest, M. Yu, J. Ruhl, Z. Tatalovich, A. Mariotto, D.R. Lewis, H.S. Chen, E.J. Feuer, and K.A. Cronin, eds. (2018). SEER Cancer Statistics Review, 1975-2015. https://seer.cancer.gov/csr/1975_2015/.

7. He, C., Poon, C., Chan, C., Yamada, S.D., and Lin, W. (2016). Nanoscale coordination polymers codeliver chemotherapeutics and siRNAs to eradicate tumors of cisplatin-resistant ovarian cancer. J. Am. Chem. Soc. *138*, 6010–6019.

8. Deng, Z.J., Morton, S.W., Ben-Akiva, E., Dreaden, E.C., Shopsowitz, K.E., and Hammond, P.T. (2013). Layer-by-layer nanoparticles for systemic codelivery of an anticancer drug and siRNA for potential triple-negative breast cancer treatment. ACS Nano *7*, 9571–9584.

9. Sudo, H., Tsuji, A.B., Sugyo, A., Ogawa, Y., Sagara, M., and Saga, T. (2012). ZDHHC8 knockdown enhances radiosensitivity and suppresses tumor growth in a mesothelioma mouse model. Cancer Sci. *103*, 203–209.

10. Dykxhoorn, D.M., Palliser, D., and Lieberman, J. (2006). The silent treatment: siRNAs as small molecule drugs. Gene Ther. *13*, 541–552.

11. Whitehead, K.A., Langer, R., and Anderson, D.G. (2009). Knocking down barriers: advances in siRNA delivery. Nat. Rev. Drug Discov. *8*, 129–138.

12. Bobbin, M.L., and Rossi, J.J. (2016). RNA interference (RNAi)-based therapeutics: delivering on the promise? Annu. Rev. Pharmacol. Toxicol. *56*, 103–122.

13. Dominska, M., and Dykxhoorn, D.M. (2010). Breaking down the barriers: siRNA delivery and endosome escape. J. Cell Sci. *123*, 1183–1189.

14. Karnofsky, D.A. (1968). Mechanism of action of anticancer drugs at a cellular level. CA Cancer J. Clin. *18*, 232–234.

15. Wu, S.Y., Lopez-Berestein, G., Calin, G.A., and Sood, A.K. (2014). RNAi therapies: drugging the undruggable. Sci. Transl. Med. *6*, 240ps7.

16. Miele, E., Spinelli, G.P., Miele, E., Di Fabrizio, E., Ferretti, E., Tomao, S., and Gulino, A. (2012). Nanoparticle-based delivery of small interfering RNA: challenges for cancer therapy. Int. J. Nanomed. *7*, 3637–3657.

17. Watts, J.K., Deleavey, G.F., and Damha, M.J. (2008). Chemically modified siRNA: tools and applications. Drug Discov. Today *13*, 842–855.

18. Chiu, Y.L., and Rana, T.M. (2003). siRNA function in RNAi: a chemical modification analysis. RNA *9*, 1034–1048.

19. Czauderna, F., Fechtner, M., Dames, S., Aygün, H., Klippel, A., Pronk, G.J., Giese, K., and Kaufmann, J. (2003). Structural variations and stabilising modifications of synthetic siRNAs in mammalian cells. Nucleic Acids Res. *31*, 2705–2716.

20. Amarzguioui, M., Holen, T., Babaie, E., and Prydz, H. (2003). Tolerance for mutations and chemical modifications in a siRNA. Nucleic Acids Res. *31*, 589–595.

21. Collingwood, M.A., Rose, S.D., Huang, L., Hillier, C., Amarzguioui, M., Wiiger, M.T., Soifer, H.S., Rossi, J.J., and Behlke, M.A. (2008). Chemical modification patterns compatible with high potency dicer-substrate small interfering RNAs. Oligonucleotides *18*, 187–200.

22. Cun, D., Jensen, D.K., Maltesen, M.J., Bunker, M., Whiteside, P., Scurr, D., Foged, C., and Nielsen, H.M. (2011). High loading efficiency and sustained release of siRNA encapsulated in PLGA nanoparticles: quality by design optimization and characterization. Eur. J. Pharm. Biopharm. *77*, 26–35.

23. Bartlett, D.W., Su, H., Hildebrandt, I.J., Weber, W.A., and Davis, M.E. (2007). Impact of tumor-specific targeting on the biodistribution and efficacy of siRNA nanoparticles measured by multimodality in vivo imaging. Proc. Natl. Acad. Sci. USA *104*, 15549–15554.

24. Schroeder, A., Levins, C.G., Cortez, C., Langer, R., and Anderson, D.G. (2010). Lipid-based nanotherapeutics for siRNA delivery. J. Intern. Med. *267*, 9–21.

25. Jang, M., Kim, J.H., Nam, H.Y., Kwon, I.C., and Ahn, H.J. (2015). Design of a platform technology for systemic delivery of siRNA to tumours using rolling circle transcription. Nat. Commun. *6*, 7930.

26. Patil, Y., and Panyam, J. (2009). Polymeric nanoparticles for siRNA delivery and gene silencing. Int. J. Pharm. *367*, 195–203.

27. Horcajada, P., Gref, R., Baati, T., Allan, P.K., Maurin, G., Couvreur, P., Férey, G., Morris, R.E., and Serre, C. (2012). Metal-organic frameworks in biomedicine. Chem. Rev. *112*, 1232–1268.

28. Xiao, B., Wheatley, P.S., Zhao, X., Fletcher, A.J., Fox, S., Rossi, A.G., Megson, I.L., Bordiga, S., Regli, L., Thomas, K.M., et al. (2007). High-capacity hydrogen and nitric oxide adsorption and storage in a metal−organic framework. J. Am. Chem. Soc. *129*, 1203–1209.

29. He, C., Lu, K., Liu, D., and Lin, W. (2014). Nanoscale metal-organic frameworks for the co-delivery of cisplatin and pooled siRNAs to enhance therapeutic efficacy in drug-resistant ovarian cancer cells. J. Am. Chem. Soc. *136*, 5181–5184.

30. Horcajada, P., Chalati, T., Serre, C., Gillet, B., Sebrie, C., Baati, T., Eubank, J.F., Heurtaux, D., Clayette, P., Kreuz, C., et al. (2010). Porous metal-organic-framework nanoscale carriers as a potential platform for drug delivery and imaging. Nat. Mater. *9*, 172–178.

31. Teplensky, M.H., Fantham, M., Li, P., Wang, T.C., Mehta, J.P., Young, L.J., Moghadam, P.Z., Hupp, J.T., Farha, O.K., Kaminski, C.F., et al. (2017). Temperature treatment of highly porous zirconium-containing metal-organic frameworks extends drug delivery release. J. Am. Chem. Soc. *139*, 7522–7532.

32. Alsaiari, S.K., Patil, S., Alyami, M., Alamoudi, K.O., Aleisa, F.A., Merzaban, J.S., Li, M., and Khashab, N.M. (2018). Endosomal escape and delivery of CRISPR/Cas9 genome editing machinery enabled by nanoscale zeolitic imidazolate framework. J. Am. Chem. Soc. *140*, 143–146.

33. Chen, Q., Xu, M., Zheng, W., Xu, T., Deng, H., and Liu, J. (2017). Se/Ru-decorated porous metal-organic framework nanoparticles for the delivery of pooled siRNAs to reversing multidrug resistance in Taxol-resistant breast cancer cells. ACS Appl. Mater. Interfaces *9*, 6712–6724.

34. Tamames-Tabar, C., Cunha, D., Imbuluzqueta, E., Ragon, F., Serre, C., Blanco-Prieto, M.J., and Horcajada, P. (2014). Cytotoxicity of nanoscaled metal-organic frameworks. J. Mater. Chem. B *2*, 262–271.

35. Abánades Lázaro, I., Haddad, S., Sacca, S., Orellana-Tavra, C., Fairen-Jimenez, D., and Forgan, R.S. (2017). Selective surface pegylation of UiO-66 nanoparticles for enhanced stability, cell uptake, and pH-responsive drug delivery. Chem *2*, 561–578.

36. Orellana-Tavra, C., Baxter, E.F., Tian, T., Bennett, T.D., Slater, N.K.H., Cheetham, A.K., and Fairen-Jimenez, D. (2015). Amorphous metal-organic frameworks for drug delivery. Chem. Commun. (Camb.) *51*, 13878–13881.

37. Howarth, A.J., Liu, Y., Li, P., Li, Z., Wang, T.C., Hupp, J.T., and Farha, O.K. (2016). Chemical, thermal and mechanical stabilities of metal-organic frameworks. Nat. Rev. Mater. *1*, 15018.

38. Mondloch, J.E., Bury, W., Fairen-Jimenez, D., Kwon, S., DeMarco, E.J., Weston, M.H., Sarjeant, A.A., Nguyen, S.T., Stair, P.C., Snurr, R.Q., et al. (2013). Vapor-phase metalation by atomic layer deposition in a metal-organic framework. J. Am. Chem. Soc. *135*, 10294–10297.

39. Cavka, J.H., Jakobsen, S., Olsbye, U., Guillou, N., Lamberti, C., Bordiga, S., and Lillerud, K.P. (2008). A new zirconium inorganic building brick forming metal organic frameworks with exceptional stability. J. Am. Chem. Soc. *130*, 13850–13851.

40. Lu, M., Williamson, N., Mishra, A., Michel, C.H., Kaminski, C.F., Tunnacliffe, A., and Kaminski Schierle, G.S. (2019). Structural progression of amyloid-β Arctic mutant aggregation in cells revealed by multiparametric imaging. J. Biol. Chem. *294*, 1478–1487.

41. Thermo Fisher Scientific. siRNA design guidelines. Technical Bulletin #506. https://www.thermofisher.com/uk/en/home/references/ambion-tech-support/rnai-sirna/general-articles/-sirna-design-guidelines.html.

42. Sabel, J.; Integrated DNA Technologies. RNAi and DsiRNA: pathway, mechanism, and design. http://www.idtdna.com/pages/education/decoded/article/rnai.

43. Islamoglu, T., Otake, K.-I., Li, P., Buru, C.T., Peters, A.W., Akpinar, I., Garibay, S.J., and Farha, O.K. (2018). Revisiting the structural homogeneity of NU-1000, a Zr-based metal–organic framework. CrystEngComm *20*, 5913–5918.

44. Suhling, K., Hirvonen, L.M., Levitt, J.A., Chung, P.-H., Tregidgo, C., Le Marois, A., Rusakov, D.A., Zheng, K., Ameer-Beg, S., Poland, S., et al. (2015). Fluorescence lifetime imaging (FLIM): basic concepts and some recent developments. Med. Photonics *27*, 3–40.

45. Cervia, L.D., Chang, C.C., Wang, L., and Yuan, F. (2017). Distinct effects of endosomal escape and inhibition of endosomal trafficking on gene delivery via electrotransfection. PLoS One *12*, e0171699.

46. Varkouhi, A.K., Scholte, M., Storm, G., and Haisma, H.J. (2011). Endosomal escape pathways for delivery of biologicals. J. Control. Release *151*, 220–228.

47. Ströhl, F., and Kaminski, C.F. (2016). Frontiers in structured illumination microscopy. Optica *3*, 667.

48. Li, P., Moon, S.Y., Guelta, M.A., Lin, L., Gómez-Gualdrón, D.A., Snurr, R.Q., Harvey, S.P., Hupp, J.T., and Farha, O.K. (2016). Nanosizing a metal-organic framework enzyme carrier for accelerating nerve agent hydrolysis. ACS Nano *10*, 9174–9182.

49. Dassault Systèmes BIOVIA, Materials Studio, v7.0, San Diego: Dassault Systèmes, 2019.

50. Rappe, A.K., Casewit, C.J., Colwell, K.S., Goddard, W.A., and Skiff, W.M. (1992). UFF, a full periodic table force field for molecular mechanics and molecular dynamics simulations. J. Am. Chem. Soc. *114*, 10024–10035.

51. Frank, J.H., Elder, A.D., Swartling, J., Venkitaraman, A.R., Jeyasekharan, A.D., and Kaminski, C.F. (2007). A white light confocal microscope for spectrally resolved multidimensional imaging. J. Microsc. *227*, 203–215.

52. Warren, S.C., Margineanu, A., Alibhai, D., Kelly, D.J., Talbot, C., Alexandrov, Y., Munro, I., Katan, M., Dunsby, C., and French, P.M.W. (2013). Rapid global fitting of large fluorescence lifetime imaging microscopy datasets. PLoS One *8*, e70687.

53. Young, L.J., Ströhl, F., and Kaminski, C.F. (2016). A guide to structured illumination TIRF microscopy at high speed with multiple colors. J. Vis. Exp. e53988.

54. Müller, M., Mönkemöller, V., Hennig, S., Hübner, W., and Huser, T. (2016). Open-source image reconstruction of super-resolution structured illumination microscopy data in ImageJ. Nat. Commun. *7*, 10980.